RESEARCH ARTICLE
doi: 10.2306/scienceasia1513-1874.2024.s005

ScienceAsia 50S (1): 2024: ID 2024s005: **1–10**

Flow injection amperometric sensor based on reduced graphene oxide modified electrode for continuous salicylic acid detection

Supapich Romportong[a,b,c], **Apon Numnuam**[a,b,c], **Natha Nontipichet**[a], **Thanawath Tuntiwongmetee**[a,b,c], **Panote Thavarungkul**[a,b,c], **Proespichaya Kanatharana**[a,b,c], **Suntisak Khumngern**[a,*]

[a] Center of Excellence for Trace Analysis and Biosensor, Faculty of Science, Prince of Songkla University, Songkhla 90110 Thailand
[b] Division of Physical Science, Faculty of Science, Prince of Songkla University, Songkhla 90110 Thailand
[c] Center of Excellence for Innovation in Chemistry, Faculty of Science, Prince of Songkla University, Songkhla 90110 Thailand

*Corresponding author, e-mail: suntisak.k@psu.ac.th

Received 26 Jan 2024, Accepted 7 Oct 2024
Available online 10 Nov 2024

ABSTRACT: Salicylic acid (SA) is widely used in cosmetics and medicine for its anti-inflammatory, antimicrobial, and antifungal properties. Excessive exposure to SA may cause vomiting, skin irritation, headaches, and increased blood pressure. In this study, an electrochemical SA sensor was developed by modifying a screen-printed carbon electrode with reduced graphene oxide (rGO/SPCE). The surface morphology of the rGO/SPCE was characterized using scanning electron microscopy (SEM). Ultraviolet-visible (UV-Vis) spectrophotometry, and Fourier-transform infrared (FT-IR) spectroscopy were also performed to confirm the structural properties of the electrode materials. Electrochemical behaviors of rGO/SPCE toward SA were characterized by cyclic voltammetry. SA was determined at the detection potential of +0.55 V by an amperometric method coupled with a flow injection system. Under optimum conditions, the SA sensor provided a wide linear range of 2.0 µmol/l to 1.0 mmol/l, a detection limit of 0.69 µmol/l, and a short analysis time (1 min). Stability, reproducibility, and selectivity of the developed sensor were excellent. The modified electrode could be used for over 91 detections. The developed sensor detected SA in cosmetic and pharmaceutical samples with a recovery range of 92.1–102.4%, indicating that the method was highly accurate. In addition, the obtained results of SA levels agreed with those obtained by UV-Vis spectrophotometry. Therefore, the developed sensor offers a reliable electrochemical strategy for the detection of SA.

KEYWORDS: electrochemical sensor, flow injection analysis, salicylic acid, reduced graphene oxide

INTRODUCTION

Salicylic acid (SA), or 2-hydroxybenzoic acid, is commonly found in a group of phenolic compounds consisting of an aromatic ring bearing a hydroxyl group or its functional derivative [1]. SA is synthesized by plants and is used in medical, cosmetic, and clinical products because it helps to slough off dead skin cells and has anti-inflammatory, antimicrobial, and antifungal properties [2]. However, excessive SA may cause problems such as vomiting, skin irritation, headaches, and increased blood pressure [3]. The Food and Drug Administration (FDA) has reported that the maximum safe concentration of SA in cosmetic products is 2.0% [4]. Moreover, SA is also a primary hydrolysate of acetylsalicylate, or aspirin, which is widely used as an anti-inflammatory medicine [5]. Therefore, the sensitive and selective determination of SA is of some importance.

Current analytical methods of SA determination include spectrophotometry [6], high-performance liquid chromatography [7], fluorimetry [8], and colorimetry [9]. Unfortunately, most of the aforementioned methods require professional expertise, complicated procedures, and considerable expenses. Hence, the development of a simple, sensitive, low-cost, and accurate method of detecting SA is necessary. Electroanalytical techniques are simple, sensitive, and low-cost methods of determining various analytes [10, 11]. Nonetheless, the direct electrochemical oxidation of SA at a conventional working electrode is difficult due to the slow electron transfer rate [12]. Consequently, the electrode must be modified to enhance the electrochemical reaction of SA.

Carbon nanomaterials have been used to improve the performances of electrochemical sensors [13]. They possess the advantages of good chemical and mechanical stability, high electrical conductivity, and low cost making them promising materials for electroanalysis [14, 15]. Carbon dots [16], carbon nanohorns [17], carbon nanotubes [11], and graphene [18, 19] are examples of carbon nanomaterials that have been used as sensing materials. Additionally, carbon quantum dots and graphene were also used in the fields of drug carriers in biomedicine [20] and energy storage [21]. Reduced graphene oxide (rGO) has also gained a lot of attention due to its conjugated π structure of sp^2 hybridized carbon atoms and has been used to enhance electron transfer by providing a large surface area and excellent electrical conductivity [22].

In the present study, we developed an electrochemical SA sensor based on a screen-printed carbon electrode modified with rGO (rGO/SPCE). A flow injection analysis (FIA) system was integrated with electrochemical detection to improve analytical performances. FIA can improve resolution manipulation, assay repeatability, speed detection, and enabling continuous measurement [23, 24]. To obtain the best analytical performances, the condition of SA determination was optimized to improve sensor sensitivity. Relevant parameters included the amount of rGO dropped on the working electrode, operating potential, flow rate, and sample volume. The analytical performances of the rGO/SPCE toward SA detection were then evaluated. Finally, the developed sensor was applied to determine SA levels in a cosmetic product. Also, aspirin was determined as an SA derivative after hydrolysis in an alkaline condition.

MATERIALS AND METHODS

Chemicals

SA, starch, benzoic acid (BA), ascorbic acid (AA), L-cysteine (L-cys), and graphene oxide (GO) were obtained from Sigma-Aldrich (Steinheim, Germany). rGO (surface area 600–750 m^2/g) was from Cheap Tubes Inc. (Brattleboro, USA). Sodium hydroxide and potassium chloride were from Merck (Darmstadt, Germany). Citric acid (CA) was from Ajax Finechem (Sydney, Australia). Zinc chloride was purchased from Kemaus (Cherrybrrook, Australia). All other chemicals were of analytical grade, and all solutions were prepared with deionized (DI) water.

Apparatus

All electrochemical measurements were conducted using a μStat 8000 multi-potentiostat/galvanostat (Metrohm-Dropsens, Switzerland) and controlled using Drop View 8400 software. The SPCE (PICS Corp., Taiwan) comprised a carbon working electrode, a silver pseudo-reference electrode, and a carbon counter electrode. Electrode surface morphology was examined using a scanning electron microscope (SEM) (Quanta 400, FEI, USA). Ultraviolet-visible spectrophotometer (Thermo Scientific™ GENESYS™ 150 UV-Vis Spectroscopy, USA) and Fourier-transform infrared (FT-IR) spectroscopy (Thermo Scientific Nicolet™ iS5 FT-IR spectrometer, UK) were used for the characterization of GO and rGO. The FIA system for continuous amperometric measurement used a Minipuls peristaltic pump (Gilson, France) to continuously flow carrier buffer into the flow cell. A custom-built screen-printed electrode flow cell with a fixed detection volume of 10 μl was used. SA standards and samples were injected at the desired volume and flow rate (see Optimization section) by a six-port valve (Valco Instrument, USA).

Fabrication of rGO/SPCE

The SA sensor was prepared by modifying the carbon working electrode of the SPCE (Fig. 1(a)). A 1.0 mg/ml rGO suspension was prepared by dispersing rGO in DI water. The SPCE was then modified by dropping 3.0 μl of rGO suspension on the working electrode surface. The modified electrode was dried under an infrared lamp to obtain the rGO/SPCE. A GO/SPCE was fabricated in the same way for comparison.

Electrochemical measurement

Electrochemical characterizations of the bare SPCE, the GO/SPCE, and the rGO/SPCE were performed using cyclic voltammetry (CV) at a scan rate of 100 mV/s in a 1.0 mmol/l $Fe(CN)_6^{3-}$ solution containing 0.10 mol/l KCl. The electrochemical behavior of the modified electrodes towards SA oxidation was examined using CV in 0.10 mol/l NaOH. Amperometric measurements were performed in the FIA system using NaOH as the carrier solution (Fig. 1(b)).

Real sample detection

Acne gels and aspirin were tested. Prior to analysis with the developed electrochemical sensor, 0.5500 g of acne gel was dissolved in 25.00 ml of 0.10 mol/l NaOH, and an aspirin tablet of 0.0970 g was dissolved in 10.00 ml of 0.10 mol/l NaOH. After that, samples were then diluted 100 times for acne gels and 1,000 times for aspirin to minimize the matrix effect and to ensure they fell within the detection concentration range of the proposed sensor. For comparison, the SA content in real samples was determined by UV-Vis spectrophotometry [25].

RESULTS AND DISCUSSION

Morphological characterization of the modified electrodes

The surface morphologies of the bare SPCE and the rGO/SPCE were characterized by SEM. The carbon working electrode of the bare SPCE presented a smooth compacted carbon layer (Fig. 2(a)). The surface of the working electrode of the rGO/SPCE (Fig. 2(b)) was covered with a uniform distribution of rGO sheets, which created a rougher surface and confirmed that the modification of the SPCE with rGO was successful. The surface morphology of the modified electrode produced a larger active surface area and was, therefore, expected to produce favorable electrochemical properties such as higher conductivity and faster electron transfer, towards SA oxidation.

Characterization of GO and rGO

UV-vis spectrophotometry was employed to estimate the transitions of the chromophores in the sample from the ground state to the excited state by analyzing the absorption spectra of GO and rGO. The maximum absorption peak of the $\pi \rightarrow \pi^*$ transition at 244 nm

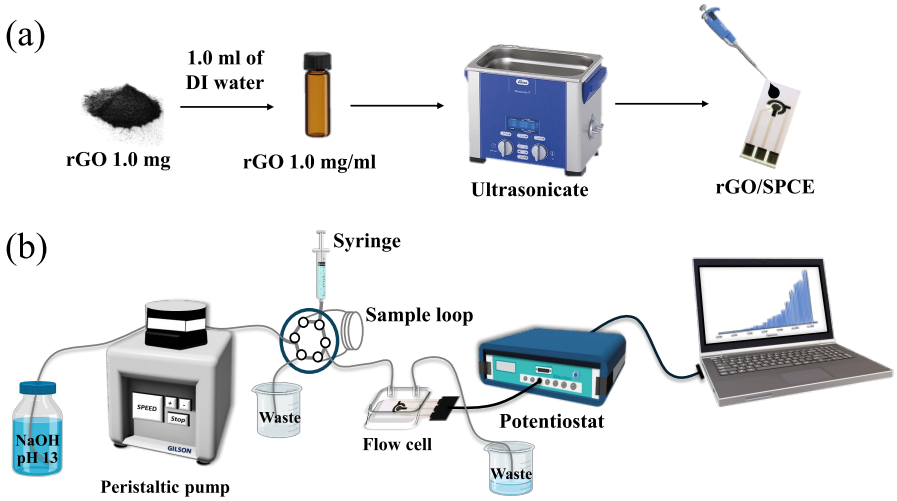

Fig. 1 (a), Schematics of the rGO/SPCE preparation; (b), the flow injection amperometric system for SA detection.

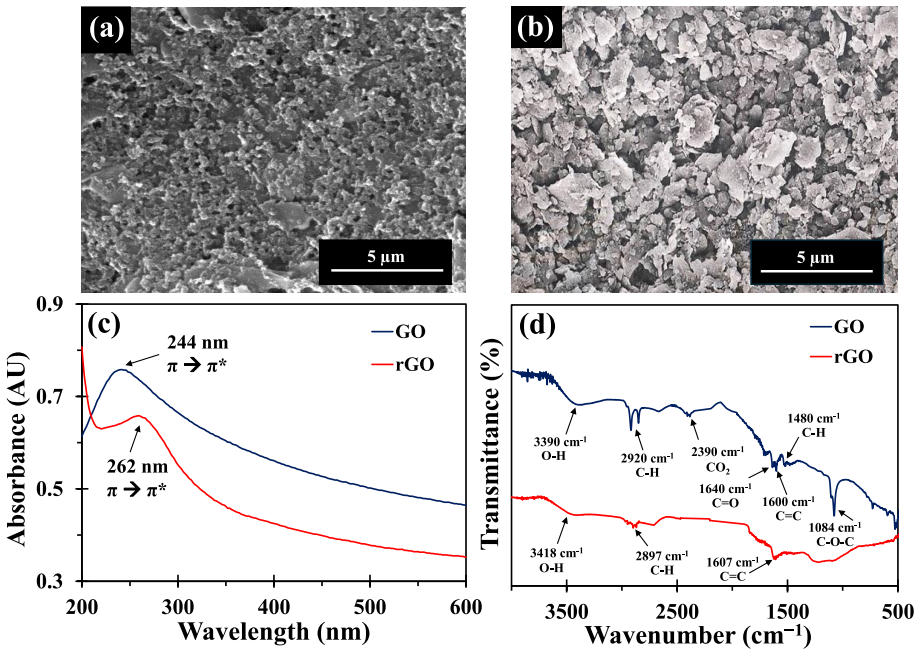

Fig. 2 (a) and (b), SEM images of a bare SPCE and a rGO/SPCE, respectively, at a 10,000× magnification; (c), UV-vis spectra; and (d), FT-IR spectra of GO and rGO.

was observed in the GO (Fig. 2(c)) [26]. In contrast, the peak of rGO shifted to 262 nm, suggesting that functional groups present on the GO surface had been removed (i.e., the carboxyl group), thereby restoring the conjugated structure [27].

The functional groups of the nanomaterials were also investigated using FT-IR to further assess the GO and rGO structures. For the GO, the absorption peaks at 3390, 2920, 1640, 1600, and 1084 cm^{-1} were assigned to the stretching vibrations of O–H, C–H, C=O, C=C, and C–O, respectively (Fig. 2(d)) [28]. The aforementioned peaks served to validate the existence of carboxyl groups within the graphene structure. Moreover, the peak observed at 2390 cm^{-1} was attributed to atmospheric CO_2. Compared with the GO, the absorption spectrum of rGO did not show the characteristic peak of carboxyl groups. This finding suggested that the conjugated structure had been recovered. Thus, the conductivity and the electron transfer ability could be improved.

Electrochemical characterization

The CV response of the rGO/SPCE in 1.0 mmol/l $Fe(CN)_6^{3-}$ with 0.10 mol/l KCl showed higher redox peak currents compared with the bare SPCE and the GO/SPCE. The better response was due to the high conductivity, large active surface area, and fast electron transfer rate of rGO (Fig. 3(a)) [29]. To further assess the electrochemical properties of different electrode modifications, electron-transfer characteristics of the various electrodes were examined using EIS in a solution of 1.0 mmol/l $Fe(CN)_6^{3-/4-}$ containing 0.10 mol/l KCl. The obtained Nyquist plots of the bare SPCE, the GO/SPCE, and the rGO/SPCE were evaluated (Fig. 3(b)). According to the Randles circuit (Fig. 3(b), inset), the diameters of the plotted semicircles indicated the electron transfer resistance (R_{et}) of the modified electrode, and the linear part at the low-frequency region indicated the diffusion process. The bare SPCE displayed the R_{et} of 5300 Ω, which decreased to 3460 Ω after being modified with GO due to the conductivity enhancement. The observed R_{et} was significantly decreased to 1250 Ω, indicating the electron-transfer characteristic was improved by the high conductivity, the large active surface area, and the fast electron transfer rate of rGO.

The active surface area of the rGO-modified electrode was then studied using CV at different scan rates in 1.0 mmol/l $Fe(CN)_6^{3-}$ containing 0.10 mol/l KCl (Fig. 3(c)) and was calculated using the Randles-Sevcik equation (1) [30],

$$I_p = (2.69 \times 10^5) n^{2/3} A D^{1/2} \nu^{1/2} C, \qquad (1)$$

where I_p is the anodic peak current, n is the number of transferred electrons, A is the electroactive surface area, D is the ferricyanide diffusion coefficient, ν is the scan rate, and C is the ferricyanide concentration. The slope of the linear plot between the anodic peak current and the square root of the scan rate was 181.18 $\mu A\, s^{1/2}/V^{1/2}$. The effective surface area of the rGO/SPCE was calculated to be 0.050 cm^2.

Electrocatalytic oxidation of SA at the modified electrodes

The electrochemical behaviors towards SA oxidation of the bare SPCE, the GO/SPCE, and the rGO/SPCE were studied using CV in 0.10 mol/l NaOH. (The NaOH was used as a supporting electrolyte solution to facilitate the oxidation of SA [5].) In the presence of 2.0 mmol/l SA, no redox peak was observed at the bare SPCE. Oxidation peaks were observed at the GO/SPCE (∼ 0.45 V) and the rGO/SPCE (∼ 0.40 V) (Fig. 4(a)), indicating the electrocatalytic activity of GO and rGO towards SA oxidation and the large surface area of the modified electrodes. Significantly, the current response towards SA oxidation at the rGO/SPCE produced the highest oxidation peak due to the faster electron transfer and higher conductivity of rGO. The mechanism of SA oxidation in NaOH solution was illustrated in Fig. 4(b). SA was oxidized to carboxyl-hydroquinone at ∼ 0.40 V by releasing one electron and one proton. The simultaneous irreversible chemical oxidation of carboxyl-hydroquinone produced carboxyl-*para*-benzoquinone. This product could be indicated by a small quasi-reversible redox peak at a potential of ∼ 0.05 V, resulting from oxidation and reduction between carboxyl-hydroquinone and carboxyl-*para*-benzoquinone [31].

The amperometric response in FIA was investigated by detecting 2.0 mmol/l SA. The results showed the same trend as the CV study. The rGO/SPCE produced the highest oxidation current (Fig. 4(c)). Therefore, the rGO/SPCE was further applied to detect SA. The electrochemical oxidation of SA at the rGO/SPCE was then investigated using CV at different scan rates in the presence of 1.0 mmol/l SA (Fig. 4(d)). The anodic peak current (I_{pa}) increased linearly with the square root of the scan rate ($\nu^{1/2}$), indicating that the oxidation of SA at the rGO/SPCE was controlled by diffusion (Fig. 4(e)). Additionally, as the scan rate increased, the anodic peak potential (E_{pa}) shifted positively, indicating a charge transfer kinetics limitation in the reaction between SA and the modified electrode [32]. Therefore, the number of electrons for the oxidation of SA could be determined by plotting between the E_{pa} and the logarithm of the scan rate ($\log \nu$). The E_{pa} was linear with the $\log \nu$ (Fig. 4(f)), which followed Laviron's equation (2) [33]:

$$E_{pa} = \text{Constant} + \frac{2.303RT}{(1-\alpha)nF} \log \nu, \qquad (2)$$

where α is the charge transfer coefficient, n is the number of electron transfers, F is the Faraday constant (96,485 C/mol), T is the temperature (298 K), and R is the gas constant (8.314 J/mol K). Thus, the slope of the plot (0.092) was equal to $2.303RT/(1-\alpha)nF$. Assuming $\alpha = 0.5$, the electron involved in the rate-determining step was calculated to be ∼ 1.

Optimization

The parameters optimized to improve sensor sensitivity included the amount of rGO dropped on the SPCE, the pH of NaOH solution, the applied potential, the sample volume, and the flow rate. The optimization was performed by measuring 0.60 mmol/l SA and comparing the obtained oxidation responses. The highest oxidation current, fast detection time, and low volume of SA indicated the optimal condition.

The amount of rGO dropped on the electrode surface could affect electrocatalytic properties and change the surface area of the working electrode. The amount of rGO used in electrode modification was varied at 2.0, 3.0, and 4.0 µg. The electrode modified with 3.0 µg produced the best response, i.e., better than

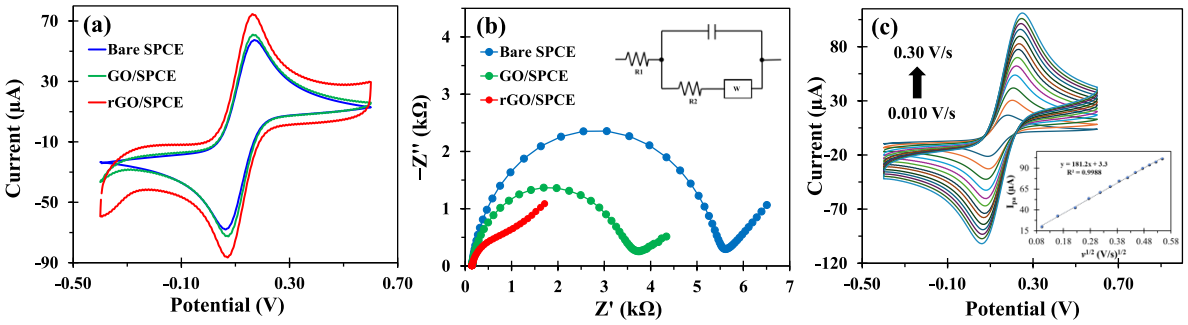

Fig. 3 (a), CVs produced in 5.0 mmol/l $Fe(CN)_6^{3-}$ solution containing 0.10 mol/l KCl at a scan rate of 100 mV/s at the bare SPCE (blue line), GO/SPCE (green line), and rGO/SPCE (red line); (b), EIS plots produced in 1.0 mmol/l $Fe(CN)_6^{3-/4-}$ solution containing 0.10 mol/l KCl at the bare SPCE (blue line), GO/SPCE (green line), and rGO/SPCE (red line); (c), CVs of the rGO/SPCE produced at different scan rates from 10 to 300 mV/s in 5.0 mmol/l $Fe(CN)_6^{3-}$ solution containing 0.10 mol/l KCl. The inset shows the linear relationship between the peak current and the square root of the scan rate.

the electrode modified with 2.0 µg current due to the increased electrical conductivity and electrode surface area, and the faster electron transfer rate (Fig. 5(a)); and better than the electrode modified with 4.0 µg due to the thickness of the rGO layer inhibiting the electron transfer. Therefore, the optimal amount of rGO was 3.0 µg.

Moreover, the electrochemical oxidation of SA was also affected by the pH of the electrolyte. The pH of NaOH, ranging from 10.0 to 14.0, was then examined. The oxidation current increased with increases of pH ranging from 10.0 to 13.0 and remained constant thereafter (Fig. 5(b)). This was due to the deprotonation of the carboxyl and phenolic groups of SA to form the salicylate ion ($pKa_1 = 2.97$, $pKa_2 = 13.4$), which is favorable for the oxidation mechanism to produce 2,5-dihydroxy benzoic acid and 2,3-dihydroxy benzoic acid [6]. It should be noted that SA was fully deprotonated and existed mainly in the deprotonated form at a pH higher than $\sim$ 13. In addition, the CV responses of 1.0 mmol/l SA in NaOH solution at different pH values were also investigated (Fig. 5(c)). With increases in the pH values, the E_{pa} of SA exhibited a negative shift, indicating the proton was involved in the oxidation reaction. The linear regression equation was $E_{pa} = -0.045\,pH + 0.96$ ($R^2 = 0.9977$) (Fig. 5(d)). The slope was close to the Nernstian theoretical value, indicating the numbers of proton and electron were equal. Therefore, the irreversible oxidation of SA participated one electron and one proton. In addition, the I_{pa} at different pH was also correlated with the flow injection amperometric response, confirming the optimal pH for detecting SA was 13.0.

The detection potential of amperometry was optimized to improve the sensitivity and selectivity of the SA sensor. The applied potential was evaluated at 0.40, 0.45, 0.50, 0.55, 0.60, and 0.65 V. The oxidation current increased with increments of applied potential from 0.40 to 0.55 V, was not significantly different at 0.60 V, and decreased at 0.65 V (Fig. 5(e)). To reduce possible interference signals from oxygen and ascorbic acid in real samples, the lower potential of 0.55 V was selected as the optimal condition.

In the FIA system, flow rate and sample volume were critical factors that affected the diffusion of SA to the electrode surface. The flow rate was studied at 0.40, 0.50, 0.55, 0.60, and 0.65 ml/min. The current response increased with flow rate increments from 0.40 to 0.60 ml/min, indicating the increased diffusion of SA to the sensor interface (Fig. 5(f)). At the highest flow rate of 0.65 ml/min, the current response was reduced due to the reduced contact time between SA and the electrode surface. The effect of sample volume was studied from 100 to 400 µl. The oxidation current was higher at 200 µl than 100 µl. At sample volumes larger than 200 µl, the current response was stable. Therefore, a flow rate of 0.60 ml/min and a sample volume of 200 µl were chosen as the optimal conditions for the determination of SA in the FIA system.

Analytical performances

Linear range and limit of detection

Analytical performances were tested under optimum conditions. The amperometric response increased with increasing concentrations of SA. A linear correlation between oxidation current and SA concentration was obtained from 2.0 µmol/l to 1.0 mmol/l (Fig. 6(a)). The limit of detection (LOD), based on the 3Sa/slope of the calibration curve, was calculated to be 0.69 µmol/l. The analytical performances of the developed sensor were compared with those of other SA sensors (Table 1). The developed sensor outperformed most reported methods by offering a wide linear range with a low LOD. Moreover, compared with previous works, the proposed electrode was simpler to fabricate.

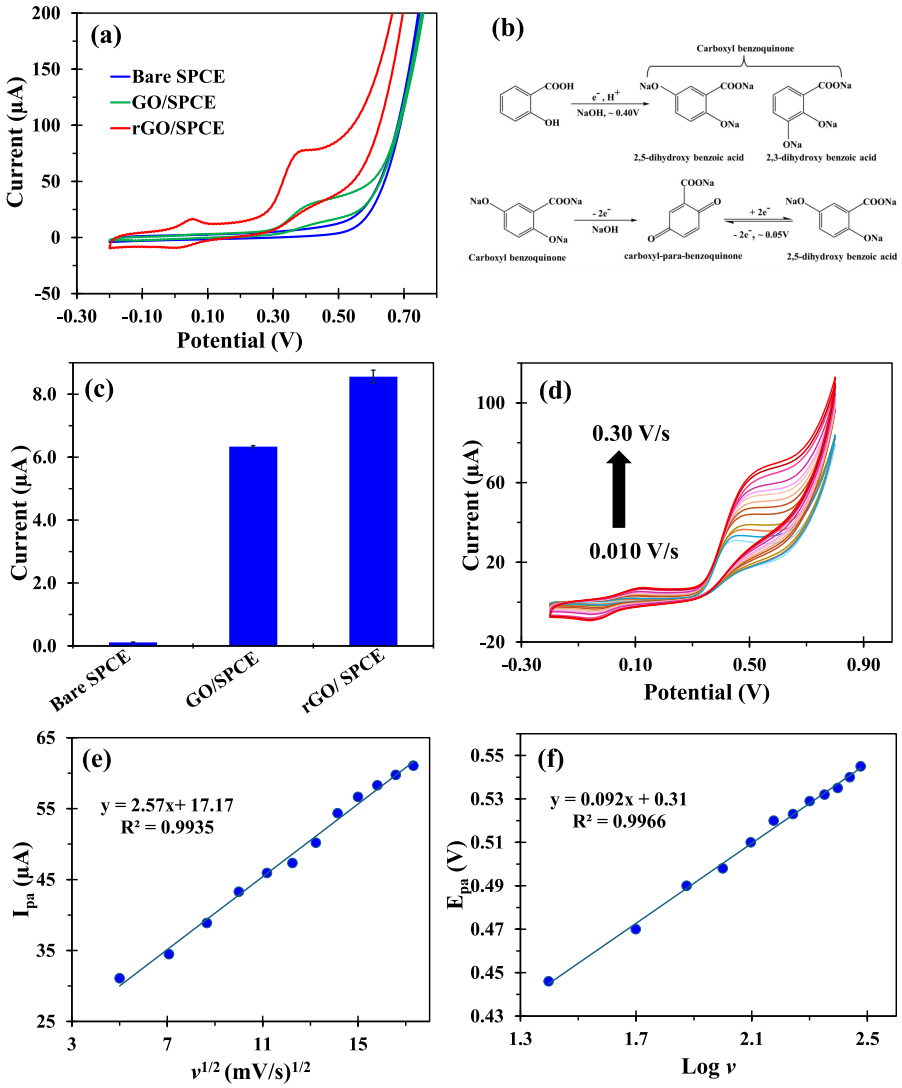

Fig. 4 (a), CVs at different modified electrodes produced at a scan rate of 100 mV/s in the presence of 2.0 mmol/l SA; (b), redox mechanism of SA; (c), sensitivities at different electrodes obtained from amperometric detection; (d), CVs produced at scan rates from 10 to 300 mV/s at a rGO/SPCE in 0.10 mol/l NaOH containing 1.0 mmol/l SA; (e), plot of anodic peak current (I_{pa}) against the square root of the scan rate ($v^{1/2}$); and (f), plot of anodic peak potential (E_{pa}) against the log of the scan rates ($\log v$).

Table 1 A comparison of the analytical performances of SA sensors.

Type of sensor	Method	Linear range (μmol/l)	LOD (μmol/l)	Ref.
CB-MWCNTs-Nafion/Fc/CB-MWCNTs/GCE	DPV	25–1000	3.30	[34]
PPRONPs–CDs–MWCNTs/GCE	DPV	0.2–60	0.1	[35]
Co/Al HTLC/Pt electrode	DPV	10–500	6.0	[12]
GO/GCE	DPV	25–2250	10	[36]
Bare SPCE	DPV	1.0–200	1.6	[37]
Anodized SPCE	SWV	16–300	5.6	[38]
rGO/SPCE	Amperometry	2.0–1000	0.69	This work

CB, carbon black; Fc, Ferrocene; PPRONPs, poly(L-proline) nanoparticles; CDs, Carbon dots; MWCNTs, multiwalled carbon nanotubes; Co/Al HTLC, Co/Al hydrotalcite; Pt, platinum; DPV, differential pulse voltammetry; SWV, square wave voltammetry.

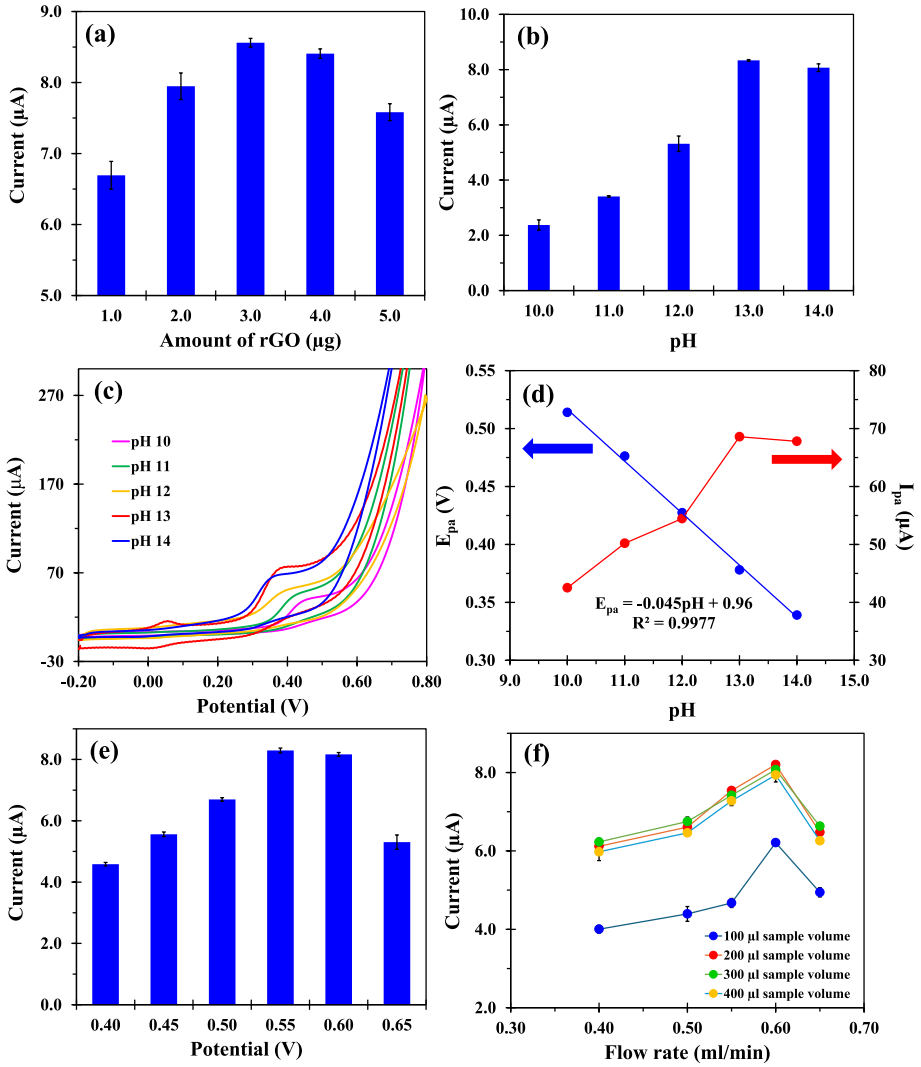

Fig. 5 (a) and (b), Oxidation current responses for detecting 0.60 mmol/l SA using FIA at electrodes modified with different amounts of rGO and different carrier solution pH values, respectively; (c), CVs produced in 0.10 mol/l NaOH solution at a scan rate of 100 mV/s at different electrolyte pH values from 10.0 to 14.0 in the presence of 1.0 mmol/l SA; (d), relation between the oxidation peak potential and the oxidation peak current of 1.0 mmol/l SA in 0.10 mol/l NaOH solution at pH 10.0 to 14.0 at a scan rate of 100 mV/s; (e), oxidation current response for detecting 0.60 mmol/l SA using FIA at different detection potentials; (f) oxidation current responses at different flow rates and sample volumes for detecting 0.60 mmol/l SA using FIA.

Operational stability and reproducibility

The stability of the fabricated SA sensor was studied by continuously detecting 0.60 mmol/l SA. Successive oxidation current responses were compared with the initial measurement. As the number of injections increased, a decrease in the current response was observed. This was due to the loss of rGO on the electrode surface during continuous measurement in the FIA system, which caused a decrease in current response. The fabricated SA sensor performed well for up to 91 injections of 0.60 mmol/l SA, producing relative responses of more than 90% (Fig. 6(b)). Note that the relative response was 80% at 157 injections. To evaluate the reproducibility of the electrode, six fabricated electrodes were prepared at different times and used to measure 0.60 mmol/l SA (Fig. 6(c)). The relative standard deviation (RSD) of the responses from six electrodes was 0.65%, indicating good electrode reproducibility.

Selectivity

The selectivity of the proposed method was investigated against starch, BA, AA, CA, L-cys, $ZnCl_2$, and KCl at 0.40 mmol/l. The responses of individual inter-

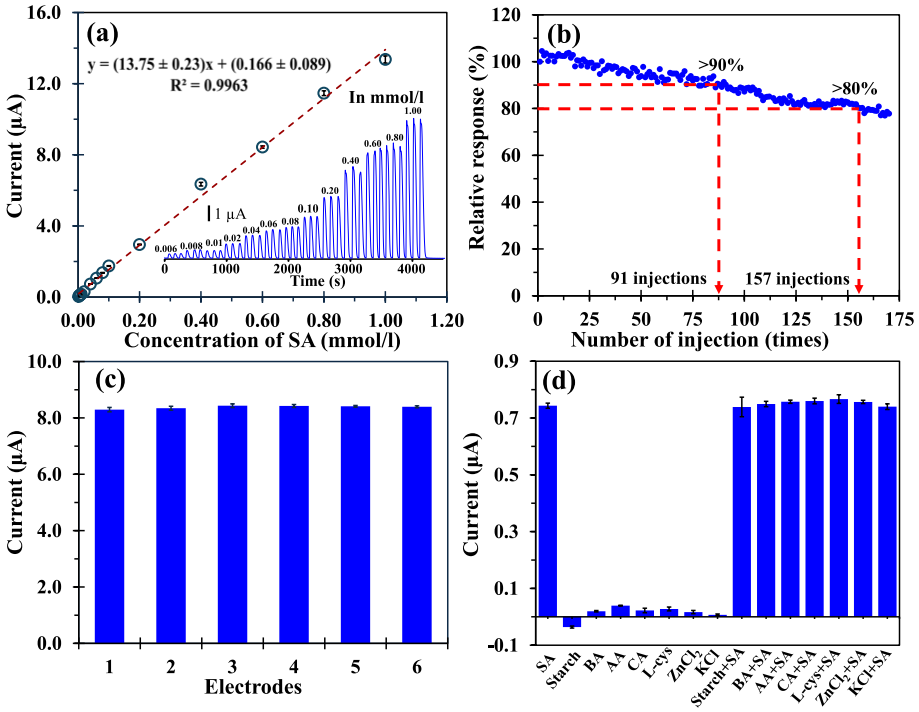

Fig. 6 (a), Calibration curve of the developed electrochemical SA sensor with the inset showing a typical amperogram of a series of SA concentrations; (b), operational stability of the developed SA sensor investigated with repeated injections of 0.60 mmol/l SA; (c), current signals of 0.60 mmol/l SA obtained from six fabricated SA sensors; (d), selectivity study of the developed SA sensor in the presence of possible interferences, including starch, BA, AA, CA, L-cys, $ZnCl_2$, and KCl at 0.40 mmol/l with SA at 0.040 mmol/l.

fering compounds were compared with the response of 0.040 mmol/l SA (Fig. 6(d)). No signals were observed for starch, BA, AA, CA, L-cys, $ZnCl_2$, and KCl. Moreover, the responses of SA mixed with each interference were not significantly different from the response of 0.040 mmol/l SA. These results indicated that the selectivity of the developed sensor was excellent for SA detection.

Real sample analysis

The developed sensor was applied to measure SA in acne gels and aspirin. The concentration of SA was measured using the standard addition methodology. The tested acne gels and aspirin samples were diluted 100 and 1,000 times, respectively, to reduce the matrix effect and to obtain a value falling within the detection range. Recoveries of spiked samples ranged from 97.9 to 102.4% for acne gels and 92.1 to 100.1% for aspirin (Table 2), indicating the developed sensor's good accuracy. RSDs were 0.09 to 3.39% for acne gels and 0.52 to 6.95% for aspirin, indicating good detection precision. Moreover, when the SA detected by the sensor was compared with the results obtained from UV-Vis spectrophotometry (Table 3), all the values were not significantly different. Furthermore, the amount of aspirin, determined as an SA derivative, was also consistent with the labeled value (Table 3). Therefore, the proposed sensor reliably determined the amount of SA in acne gels and aspirin.

Table 2 Recovery study in acne gels at 100× dilution and aspirin at 1000× dilution spiked with various SA concentrations.

Samples	Spiked SA (mmol/l)	Found SA (mmol/l)	Recovery (%)	RSD ($n = 3$, %)
Acne gel 1	–	0.0083±0.0006	–	–
	0.020	0.0287±0.0006	101.8±2.4	2.30
	0.040	0.0475±0.0012	97.9±2.1	2.18
	0.060	0.0678±0.0025	99.2±3.4	3.39
	0.080	0.0902±0.0001	102.4±0.2	0.16
	0.100	0.1073±0.0001	99.0±0.1	0.09
Acne gel 2	–	0.0481±0.0015	–	–
	0.020	0.0287±0.0002	101.7±1.0	0.94
	0.040	0.0476±0.0003	98.3±0.9	0.86
	0.060	0.0683±0.0007	99.9±0.1	1.09
	0.080	0.0890±0.0006	100.9±0.7	0.72
	0.100	0.1080±0.0012	99.7±1.1	1.18
Aspirin	–	0.0584±0.0019	–	–
	0.020	0.0759±0.0018	92.1±6.4	6.95
	0.040	0.0958±0.0008	93.6±2.0	2.17
	0.060	0.1151±0.0028	94.5±4.7	4.98
	0.080	0.1332±0.0014	93.5±1.7	1.85
	0.100	0.1585±0.0005	100.1±0.5	0.52

Table 3 SA levels detected in acne gels and aspirin by the developed sensor and UV-Vis spectrophotometry.

Samples	Listed value	Amount of SA	
		Electrochemical sensor	UV-Vis spectrophotometry
Acne gel 1	NA	0.83±0.06 mmol/l	0.71±0.08 mmol/l
Acne gel 2	NA	4.80±0.15 mmol/l	4.68±0.03 mmol/l
Aspirin	81 mg	80.7±2.6 mg	78.0±2.1 mg

NA: Not available.

CONCLUSION

In summary, salicylic acid (SA) was determined by an amperometric technique in a flow injection analysis system. The sensitivity of detection was improved by using a screen-printed carbon electrode modified with reduced graphene oxide (rGO/SPCE). The rGO exhibited a large specific surface area, a large number of active sites, and high electroconductivity, which enhanced electrocatalytic activity toward SA oxidation. Combining flow injection analysis with electrochemical detection resulted in a sensitive and precise sensor that determined SA within 1 min. Under optimal conditions, the developed sensor showed a linear range from 2.0 µmol/l to 1.0 mmol/l and a detection limit of 0.69 µmol/l. The rGO/SPCE had the advantages of simplicity and stability (up to 91 injections), good reproducibility (RSD = 0.65%), and selectivity. The proposed method was successfully applied to determine SA in real samples. The obtained results from SA determination for acne gels and aspirin with the proposed method were consistent with results from the UV-Vis spectrophotometry and the labeled values. The proposed method could be used to measure the concentration of SA in cosmetics and pharmaceutical products. Additionally, the developed SA sensor could be applied to other samples, such as plants, fruit, and human blood. However, for human blood samples, the selectivity against other interfering compounds, such as histamine, human serum albumin, glucose, and uric acid, should be evaluated.

Acknowledgements: This project was funded by the National Research Council of Thailand (NRCT, N42A650252). Supapich Romportong was supported by a Graduate Fellowship (Research Assistant) from the Faculty of Science, Prince of Songkla University (Contract no. 1-2565-02-004), the Center of Excellence for Innovation in Chemistry (PERCH-CIC), the Ministry of Higher Education, Science, Research, and Innovation, and the Center of Excellence for Trace Analysis and Biosensor (TAB-CoE) at Prince of Songkla University of Thailand. We would also like to thank the Talent Management Project of Prince of Songkla University.

REFERENCES

1. Yusuf M, Hayat S, Alyemeni MN, Fariduddin Q, Ahmad A (2013) Salicylic acid: physiological roles in plants. In: Hayat S, Ahmad A, Alyemeni MN (eds) *Salicylic Acid*, Springer, Dordrecht, pp 15–30.
2. Arif T (2015) Salicylic acid as a peeling agent: a comprehensive review. *Clin Cosmet Investig Dermatol* **8**, 455–461.
3. Klessig DF, Tian M, Choi HW (2016) Multiple targets of salicylic acid and its derivatives in plants and animals. *Front Immunol* **7**, 206.
4. Olsen TG (1982) Therapy of acne. *Med Clin North Am* **66**, 851–871.
5. Zhang WD, Xu B, Hong YX, Yu YX, Ye JS, Zhang JQ (2010) Electrochemical oxidation of salicylic acid at well-aligned multiwalled carbon nanotube electrode and its detection. *J Solid State Electrochem* **14**, 1713–1718.
6. Zebbicha Y, Yahia AK, Keraghel NE, Sarah F, Islam CA, Yacine AM (2023) Validation of a simple spectrophotometric method for the rapid determination of salicylates in plasma. *J Pharmacol Toxicol Methods* **124**, 107475.
7. Kees F, Jehnich D, Grobecker H (1996) Simultaneous determination of acetylsalicylic acid and salicylic acid in human plasma by high-performance liquid chromatography. *J Chromatogr B Biomed Appl* **677**, 172–177.
8. Karin MM, Lee HS, Kim YS, Bae HS, Lee SH (2006) Analysis of salicylic acid based on the fluorescence enhancement of the As(III)–salicylic acid system. *Anal Chim Acta* **576**, 136–139.
9. El-Gindy A, Hadad GM (2012) Chemometrics in pharmaceutical analysis: an introduction, review, and future perspectives. *J AOAC Int* **95**, 609–623.
10. Shi Z, Xia L, Li G (2023) Recent progress of electrochemical sensors in food analysis. *Chemosensors* **11**, 478.
11. Saraban M, Numnuam A, Nontipichet N, Kangkamano T, Thavarungkul P, Kanatharana P, Khumngern S (2024) A disposable electrochemical caffeine sensor based on a screen-printed electrode modified with a copper-metal organic framework and functionalized multiwalled carbon nanotube nanocomposite. *New J Chem* **48**, 3638–3645.
12. Gualandi I, Scavetta E, Zappoli S, Tonelli D (2011) Electrocatalytic oxidation of salicylic acid by a cobalt hydrotalcite-like compound modified Pt electrode. *Biosens Bioelectron* **26**, 3200–3206.
13. Porto LS, Silva DN, Oliveira AE, Pereira AC, Borges KB (2020) Carbon nanomaterials: synthesis and applications to development of electrochemical sensors in determination of drugs and compounds of clinical interest. *Rev Anal Chem* **38**, 20190017.
14. Ahammad S, Lee JJ, Rahman A (2009) Electrochemical sensors based on carbon nanotubes. *Sensors* **9**, 2289–2319.
15. Adhikari BR, Govindhan M, Chen A (2015) Carbon nanomaterials based electrochemical sensors/biosensors for the sensitive detection of pharmaceutical and biological compounds. *Sensors* **15**, 22490–22508.
16. Liu JM, Lin LP, Wang XX, Lin SQ, Cai WL, Zhang LH, Zheng ZY (2012) Highly selective and sensitive detection of Cu^{2+} with lysine enhancing bovine serum albumin modified-carbon dots fluorescent probe. *Analyst* **137**, 2637–2642.
17. Liu X, Li H, Wang F, Zhu S, Wang Y, Xu G (2010) Functionalized single-walled carbon nanohorns for electrochemical biosensing. *Biosens Bioelectron* **25**, 2194–2199.

18. Georgakilas V, Tiwari JN, Kemp C, Perman JA, Bourlinos AB, Kim KS, Zboril R (2016) Noncovalent functionalization of graphene and graphene oxide for energy materials, biosensing, catalytic, and biomedical applications. *Chem Rev* **116**, 5464–5519.
19. Khumngern S, Choosang J, Kanatharana P, Thavarungkul P, Numnuam A (2024) Voltammetric sensor for an anti-cancer drug cisplatin based on bismuth nanoparticles/graphene modified glassy carbon electrode. *Talanta* **267**, 125147.
20. Yuan H, Yang H, Yuan P, Wang T, Zhou Q (2023) Carbon quantum dots as drug carriers for tumor-associated macrophage repolarization following photothermal therapy. *ScienceAsia* **49**, 627–634.
21. Chiochan P, Suktha P, Phattharasupakun N, Duangdangchote S, Suksomboom M, Tejangkura W, Sawangphruk M (2022) Li-ion batteries of Ni-rich lithium nickel cobalt aluminium oxide coupled with high-energy lithiophilic anode. *ScienceAsia* **48**, 577–587.
22. Zhou A, Bai J, Hong W, Bai H (2022) Electrochemically reduced graphene oxide: Preparation, composites, and applications. *Carbon* **191**, 301–332.
23. Kurbanoglu S, Unal MA, Ozkan SA (2018) Recent developments on electrochemical flow injection in pharmaceuticals and biologically important compounds. *Electrochim Acta* **287**, 135–148.
24. Khumngern S, Notipichet N, Thavarungkul P, Kanatharana P, Numnuam A (2024) Smartphone-enabled flow injection amperometric glucose monitoring based on a screen-printed carbon electrode modified with PEDOT@PB and a GOx@PPtNPs@MWCNTs nanocomposite. *Talanta* **277**, 126336.
25. Chockanlingam K, Binu N, Paramasivan G (2012) Efficient photocatalytic degradation of salicylic acid by bactericidal ZnO. *J Korean Chem Soc* **56**, 108–114.
26. Khune AS, Padghan V, Bongane R, Narwade VN, Dole B, Ingle NN, Tsai M-L, Hianik T, et al (2023) Highly selective chemiresistive SO2 sensor based on a reduced graphene oxide/porphyrin (rGO/TAPP) Composite. *Electron Mater* **52**, 8108–8123.
27. Sengupta I, Chakraborty S, Talukdar M, Pal SK, Chakraborty S (2018) Thermal reduction of graphene oxide: How temperature influences purity. *J Mater Res* **33**, 4113–4122.
28. Bano N, Hussain I, Naggar AA, Albassam AA (2019) Reduced graphene oxide nanocomposites for optoelectronics applications. *Appl Phys A* **125**, 215.
29. Uzun D (2021) Determination of Paracetamol based on 3-Amino-4H-1,2,4-triazole coated glassy carbon surface in pharmaceutical sample. *Electroanalysis* **33**, 1699–1706.
30. Rowley-Neale SJ, Randviir EP, Dena AS, Banks CE (2018) An overview of recent applications of reduced graphene oxide as a basis of electroanalytical sensing platforms. *Appl Mater Today* **10**, 218–226.
31. Wu F, Wang L, Wu C, Bai Y (2009) Structural characterization and electrochemical performance of lithium trivanadate synthesized by microwave sol-gel method. *Electrochim Acta* **54**, 4613–4619.
32. Torriero AA, Luco JM, Sereno L, Raba J (2004) Voltammetric determination of salicylic acid in pharmaceuticals formulations of acetylsalicylic acid. *Talanta* **62**, 247–254.
33. Laviron E (1979) General expression of the linear potential sweep voltammogram in the case of diffusionless electrochemical systems. *J Electroanal Chem Interfacial Electrochem* **101**, 19–28.
34. Hu Y, Wang X, Wang C, Hou P, Dong H, Luo B, Li A (2020) A multifunctional ratiometric electrochemical sensor for combined determination of indole-3-acetic acid and salicylic acid. *RSC Adv* **10**, 3115–3121.
35. Li M, Kuang Y, Fan Z, Qin X, Hu S, Liang Z, Liu Q, Zhang W, et al (2022) Simultaneous electrochemical sensing of indole-3-acetic acid and salicylic acid on poly(L-proline) nanoparticles-carbon dots-multiwalled carbon nanotubes composite-modified electrode. *Sensors* **22**, 2222.
36. Vadivaambigai A, Senthil PA, Kothurkar NK, Rangarajan M (2015) Graphene-oxide-based electrochemical sensor for salicylic acid. *Nanosci Nanotechnol Lett* **7**, 140–146.
37. Detpisuttitham W, Phanthong C, Ngamchana S, Rijiravanich P, Surareungchai W (2020). Electrochemical detection of salicylic acid in pickled fruit/vegetable and juice. *J Anal Test* **4**, 291–297.
38. Rawlinson S, MaLister A, Kanyong P, Davis J (2018) Rapid determination of salicylic acid at screen printed electrodes. *Microchem J* **137**, 71–77.